A UV complete model for radiative seesaw scenarios and electroweak baryogenesis based on the supersymmetric gauge theory

Shinya Kanemura,[1] Naoki Machida,[1] Tetsuo Shindou,[2] and Toshifumi Yamada[3,*]

[1]*Department of Physics, University of Toyama, 3190 Gofuku, Toyama 930-8555, Japan*
[2]*Division of Liberal Arts, Kogakuin University, 1-24-2 Shinjuku, Tokyo 163-8677, Japan*
[3]*KEK Theory Center, 1-1 Oho, Tsukuba, Ibaraki 305-0801, Japan*

(Received 12 September 2013; published 13 January 2014)

In a class of supersymmetric gauge theories with asymptotic freedom, the low-energy effective theory below the confinement scale is described by the composite superfields of the fundamental representation fields. Based on the supersymmetric gauge theory with $N_c = 2$ and $N_f = 3$ with an additional unbroken Z_2 symmetry, we propose a new model where neutrino masses, dark matter, and baryon asymmetry of the Universe can be simultaneously explained by physics below the confinement scale. This is an example for the ultraviolet complete supersymmetric extension of so-called radiative seesaw scenarios with first-order phase transition required for successful electroweak baryogenesis. We show that there are benchmark points where all the neutrino data, the lepton flavor violation data, and the LHC data are satisfied. We also briefly discuss Higgs phenomenology in this model.

DOI: 10.1103/PhysRevD.89.013005 PACS numbers: 14.60.Pq, 12.60.Jv, 12.60.Fr

I. INTRODUCTION

The discovery of the Higgs boson [1] and measurements of its properties [2] at the LHC provide us a clue to explore the essence of electroweak symmetry breaking, which is possibly described by new physics beyond the standard model (SM) at the TeV scale. On the other hand, new physics is required to explain phenomena such as neutrino oscillation, existence of dark matter (DM), and baryon asymmetry of the Universe (BAU). If the origins of these phenomena are related to the essence of the Higgs sector, they should also arise from new physics at the TeV scale. In such cases, their origins can be found at current and future collider experiments.

For example, let us consider the scenario of generating neutrino masses by the quantum effect [3–8], in which tiny neutrino masses are explained by perturbation of the dynamics at the TeV scale. There is a class of models with right-handed (RH) neutrinos which are assigned the odd parity under an additional Z_2 symmetry [5–8]. The Z_2 symmetry forces the neutrino masses to be generated only at the quantum level, giving loop suppression to the neutrino masses. Also, the lightest Z_2-odd particle can be a DM candidate if the Z_2 symmetry is unbroken. We call such scenarios radiative seesaw scenarios. The Ma model is the simplest one in such a scenario, in which neutrino masses are generated at the one-loop level by the contribution of an extra Z_2-odd $\mathrm{SU}(2)_L$ scalar doublet (inert doublet) and Z_2-odd RH neutrinos [5]. A neutral component of the inert doublet field or the lightest RH neutrino can be the DM. On the other hand, in the Aoki-Kanemura-Seto model (the AKS model) [7,8], where Z_2-odd charged and neutral singlet scalars as well as Z_2-odd RH neutrinos are added to a two Higgs doublet model, neutrino masses are induced at the three-loop level and at the same time the lightest Z_2-odd particle (the Z_2-odd neutral singlet or the RH neutrino) can be the DM. In addition, in this model, electroweak baryogenesis can be simultaneously realized due to strong first-order electroweak phase transition (1stOPT) and the CP violating phases in the Higgs sector [9].

These models of radiative seesaw scenarios have been introduced as purely phenomenological models. For example, in the AKS model, some of the coupling constants in the Higgs sector and the new Yukawa coupling constants for the RH neutrinos are of order one in order to satisfy the condition of strong 1stOPT and also to reproduce the neutrino data. Consequently, these coupling constants blow up as the energy scale increases and the Landau pole appears at the point much below the Planck scale or the GUT scale, and the model is well defined only below the Landau pole [10]. This suggests that the model is a low-energy effective description of a more fundamental theory above the cutoff scale which corresponds to the Landau pole. It is then a very interesting question what kind of a fundamental theory can lead to such a low-energy effective theory.

In this paper, we propose a concrete model of the fundamental theory whose low-energy description gives a phenomenological model [7] of radiative seesaw scenarios with electroweak baryogenesis. In this model, the origin of the Higgs force above the cutoff scale of the low-energy theory is a new gauge interaction with asymptotic freedom. In order to describe this picture, we consider the supersymmetric (SUSY) $\mathrm{SU}(N_c)$ theory with N_f flavors [11,12]. For $N_f = N_c + 1$, confinement occurs at an infrared (IR) scale

*Present address: Department of Physics and Center for Mathematics and Theoretical Physics, National Central University, Chungli, Taiwan 32001, Republic of China.

Λ_H [13]. We here consider the simplest case with $N_c = 2$ and $N_f = 3$.[1] In the low-energy effective theory below the confinement scale Λ_H, Higgs superfields $H_{ij}(\sim T_i T_j)$ appear as the composite states of the fundamental superfields $T_i (i = 1, \ldots, 6)$ which are doublets of the $\mathrm{SU}(2)_H$ gauge symmetry [14]. In order to realize radiative seesaw scenarios in the low-energy effective theory, we add elementary RH neutrino superfields $N_i^c (i = 1, \ldots, 3)$ to the model. We further impose a Z_2 symmetry to the model assuming that N_i^c and some of the T_i's are Z_2 odd. Below the confinement scale, the symmetries of the model are $\mathrm{SU}(3)_C \times \mathrm{SU}(2)_L \times \mathrm{U}(1)_Y \times Z_2$, under which fifteen Higgs superfields appear [15]. All the scalar particles required in the AKS model are included in these fifteen Higgs superfields. It is quite interesting that the complicated particle content of the AKS model is predicted by this $\mathrm{SU}(2)_H \times Z_2$ theory above the cutoff scale without any artificial assumption.

The condition of strongly 1stOPT, $\phi_c/T_c \gtrsim 1$, which is required for successful electroweak baryogenesis determines the size of the coupling constants of the Higgs potential at the electroweak scale. This property commonly results in the enhanced triple Higgs boson coupling [17,18]. The electroweak baryogenesis scenario can partially be tested by measuring the triple Higgs boson coupling at future collider experiments. By the renormalization group equation (RGE) analysis of the coupling constant, the scale of the Landau pole is evaluated as $\mathcal{O}(10)$TeV [19,20], which is identical to the confinement scale Λ_H under the naive dimensional analysis (NDA) [21].

In our model, the lightest Z_2-odd particle in the effective theory can be a DM candidate as in usual radiative seesaw scenarios. If the R parity is also imposed, there are two discrete symmetries, and a rich possibility for the multicomponent DM scenario occurs [22]. In this paper, however, we do not specify the scenario of DM. Detailed analysis for the multicomponent DM scenario will be performed in our model elsewhere [23].

We show that the neutrino masses are generated at the loop level in the low-energy effective theory of our model. It contains diagrams of both the Ma model and the AKS model. We find benchmark points in the parameter space where all the current experimental data for Higgs bosons, neutrino data, constraints of lepton flavor violation processes, and the condition of strongly 1stOPT are satisfied. We also discuss the possibility of testing this model at current and future collider experiments.

[1]This is the same choice as in the minimal SUSY fat Higgs model [11]. In this model, however, additional heavy superfields are introduced in order to make some of the unnecessary composite superfields to be very heavy. Consequently, in the low-energy effective theory of the model, two $\mathrm{SU}(2)_L$ doublet and one singlet Higgs superfields appear as composite states of fundamental superfields of the $\mathrm{SU}(2)_H$ gauge symmetry, corresponding to the field content of the nearly minimal SUSY SM (nMSSM) [16].

II. MODEL BASED ON SUSY STRONG DYNAMICS

In this section, we will briefly review a SUSY model with $\mathrm{SU}(2)_H \times Z_2$ symmetry and six chiral superfields, denoted by $T_i (i = 1, \ldots, 6)$, which are doublets of the $\mathrm{SU}(2)_H$ gauge symmetry. The superfield T_i's are also charged under the SM gauge groups $\mathrm{SU}(2)_L \times U(1)_Y$. The SM charges and Z_2 parity assignments on T_i's are given in Table I. The tree-level superpotential respecting all the gauge symmetries and the Z_2 parity is written as

$$W_{\mathrm{tree}} = m_1 T_1 T_2 + m_3 T_3 T_4 + m_5 T_5 T_6. \tag{1}$$

The $\mathrm{SU}(2)_H$ gauge coupling becomes nonperturbative at an IR scale, denoted by Λ_H. Below the scale Λ_H, the theory is described in terms of composite chiral superfields, $H'_{ij} = T_i T_j (i \neq j)$, which are singlets of $\mathrm{SU}(2)_H$. We have the following dynamically generated superpotential below Λ_H:

$$W_{\mathrm{dyn}} = -\frac{1}{\Lambda^3} \epsilon^{ijklmn} H'_{ij} H'_{kl} H'_{mn}, \tag{2}$$

where Λ is a dynamically generated scale [13]. The total effective superpotential is simply the sum of W_{dyn} and W_{tree}:

$$W_{\mathrm{eff}} = W_{\mathrm{dyn}} + W_{\mathrm{tree}} = W_{\mathrm{dyn}} + m_1 H'_{12} + m_3 H'_{34} + m_5 H'_{56}. \tag{3}$$

We cannot determine the normalization for the dynamically generated superpotential. The effective Kähler potential below the scale Λ_H is also undetermined, and so is the canonical normalization for the mesonic superfields. However, the NDA suggests the following form of the effective Kähler potential and normalization for the effective superpotential at the scale Λ_H [21]:

$$K_{\mathrm{eff}}[\Lambda_H] \simeq \frac{1}{16\pi^2 \Lambda_H^2} H'^{\dagger}_{ij} H'_{ij}, \tag{4}$$

TABLE I. The SM charges and Z_2 parity assignments on the $\mathrm{SU}(2)_H$ doublets T_i.

Superfield	$\mathrm{SU}(3)_C$	$\mathrm{SU}(2)_L$	$\mathrm{U}(1)_Y$	Z_2
$\begin{pmatrix} T_1 \\ T_2 \end{pmatrix}$	1	2	0	+1
T_3	1	1	+1/2	+1
T_4	1	1	−1/2	+1
T_5	1	1	+1/2	−1
T_6	1	1	−1/2	−1

$$W_{\rm eff}[\Lambda_H] \simeq -\frac{1}{16\pi^2\Lambda_H^3}\epsilon^{ijklmn}H'_{ij}H'_{kl}H'_{mn} + m_1 H'_{12} + m_3 H'_{34} + m_5 H'_{56}. \quad (5)$$

The canonically normalized mesonic superfields H_{ij} at the scale Λ_H are then given by

$$H_{ij} \simeq \frac{1}{4\pi\Lambda_H}H'_{ij}, \quad (6)$$

and the superpotential at the scale Λ_H is rewritten as

$$W_{\rm eff}[\Lambda_H] \simeq 4\pi\epsilon^{ijklmn}H_{ij}H_{kl}H_{mn} + 4\pi\Lambda_H m_1 H_{12} + 4\pi\Lambda_H m_3 H_{34} + 4\pi\Lambda_H m_5 H_{56}. \quad (7)$$

The basic setup explained above is the same as the one in the minimal SUSY fat Higgs model [11]. In general, fifteen mesonic superfields H_{ij} appear in the low-energy effective theory of the fundamental $SU(2)_H$ gauge theory with three flavors. In the minimal SUSY fat Higgs model, the superfields in the low-energy effective theory are made to be identical to those in the nMSSM [16] by introducing several $SU(2)_H$ singlet superfields which give masses as large as Λ_H to ten of the fifteen mesonic superfields. On the other hand, in our model, we do not introduce such additional singlets and thus all the fifteen mesonic chiral superfields remain in the effective theory below Λ_H.

We identify the fifteen mesonic chiral superfields, H_{ij}, with the MSSM Higgs doublets, H_u, H_d, and the exotic chiral superfields in an extended Higgs sector, as

$$H_u \equiv \begin{pmatrix} H_{13} \\ H_{23} \end{pmatrix}, \quad H_d \equiv \begin{pmatrix} H_{14} \\ H_{24} \end{pmatrix}, \quad \Phi_u \equiv \begin{pmatrix} H_{15} \\ H_{25} \end{pmatrix}, \quad \Phi_d \equiv \begin{pmatrix} H_{16} \\ H_{26} \end{pmatrix}, \quad N \equiv H_{56}, \quad N_\Phi \equiv H_{34}, \quad N_\Omega \equiv H_{12}, \quad \Omega^+ \equiv H_{35}, \quad \Omega^- \equiv H_{46}, \quad \zeta \equiv H_{36}, \quad \eta \equiv H_{45}. \quad (8)$$

The SM charge and Z_2 parity of these Higgs superfields are summarized in Table II. With these fields, the superpotential in Eq. (7) is rewritten as

$$W_{\rm eff} = \hat{\lambda}\{N(H_u H_d + v_0^2) + N_\Phi(\Phi_u\Phi_d + v_\Phi^2) + N_\Omega(\Omega^+\Omega^- + v_\Omega^2) - NN_\Phi N_\Omega - N_\Omega\zeta\eta + \zeta H_d\Phi_u + \eta H_u\Phi_d - \Omega^+ H_d\Phi_d - \Omega^- H_u\Phi_u\}. \quad (9)$$

After the Z_2-even neutral fields N, N_Φ, and N_Ω get vacuum expectation values (VEVs), the relevant terms of the effective superpotential are given by [15,20]

$$W_{\rm eff} = -\mu H_u H_d - \mu_\Phi\Phi_u\Phi_d - \mu_\Omega(\Omega^+\Omega^- - \zeta\eta) + \hat{\lambda}\{H_d\Phi_u\zeta + H_u\Phi_d\eta - H_u\Phi_u\Omega^- - H_d\Phi_d\Omega^+\}. \quad (10)$$

The relevant soft SUSY breaking terms are given by

$$\mathcal{L}_H = -m_{H_u}^2 H_u^\dagger H_u - m_{H_d}^2 H_d^\dagger H_d - m_{\Phi_u}^2\Phi_u^\dagger\Phi_u - m_{\Phi_d}^2\Phi_d^\dagger\Phi_d - m_{\Omega^+}^2\Omega^{+\dagger}\Omega^+ - m_{\Omega^-}^2\Omega^{-\dagger}\Omega^- - m_\zeta^2\zeta^\dagger\zeta - m_\eta^2\eta^\dagger\eta - \{B\mu H_u H_d + B_\Phi\mu_\Phi\Phi_u\Phi_d + B_\Omega\mu_\Omega(\Omega^+\Omega^- + \zeta\eta) + \text{H.c.}\} - \{A_\zeta H_d\Phi_u\zeta + A_\eta H_u\Phi_d\eta + A_{\Omega^-}H_u\Phi_u\Omega^- + A_{\Omega^+}H_d\Phi_d\Omega^+ + \text{H.c.}\} - \left\{m_{\zeta\eta}^2\eta^\dagger\zeta + \frac{B_\zeta^2}{2}\zeta^2 + \frac{B_\eta^2}{2}\eta^2 + \text{H.c.}\right\}. \quad (11)$$

The coupling constant $\hat{\lambda}$ and the cutoff scale Λ_H are related through the NDA. Under the assumption of the NDA, the coupling constant $\hat{\lambda}$ becomes nonperturbative at Λ_H as $\hat{\lambda} \simeq 4\pi$. The value of $\hat{\lambda}$ at the cutoff scale Λ_H is connected to those at low-energy scales by RGE. Therefore, the cutoff scale Λ_H can be predicted from the value of the coupling constant $\hat{\lambda}$ at the electroweak scale, $\hat{\lambda}(\mu_{\rm EW})$. In this paper, we constrain the range of Λ_H by requiring that the coupling constant $\hat{\lambda}(\mu_{\rm EW})$ satisfies the condition of strongly 1stOPT, $\phi_c/T_c \gtrsim 1$, which is one of the conditions for successful electroweak baryogenesis [9]. In general, nondecoupling quantum effects of additional scalar fields make the order of electroweak phase transition strong. In Refs. [19,20], some of the extra scalar fields such as Φ_u, Φ_d, Ω^+, Ω^- ζ, and η significantly contribute to make the order of electroweak phase transition stronger, when the coupling $\hat{\lambda}$ satisfies $\hat{\lambda}(\mu_{\rm EW}) \gtrsim 1.6$ at the electroweak scale. Correspondingly, the Landau pole appears at the scale around ten TeV.

TABLE II. The field contents of the Higgs sector below Λ_H.

Field	$SU(3)_C$	$SU(2)_L$	$U(1)_Y$	Z_2
H_u	1	2	$+1/2$	$+1$
H_d	1	2	$-1/2$	$+1$
Φ_u	1	2	$+1/2$	-1
Φ_d	1	2	$-1/2$	-1
Ω^+	1	1	$+1$	-1
Ω^-	1	1	-1	-1
N, N_Φ, N_Ω	1	1	0	$+1$
ζ, η	1	1	0	-1

III. LOOP INDUCED NEUTRINO MASSES

We will show that radiative seesaw scenarios [5,7] are realized in the low-energy effective theory of the $SU(2)_H \times Z_2$ model by adding Z_2-odd RH neutrino superfields N_i^c. The superpotential relevant to the neutrino sector is given by

$$W_N = y_N^{ij} N_i^c L_j \Phi_u + h_N^{ij} N_i^c E_j^c \Omega^- + \frac{M_i}{2} N_i^c N_i^c, \quad (12)$$

where E_i^c and L_i are the RH charged lepton chiral superfields and the lepton doublet chiral superfield, respectively, and the basis of the lepton fields is taken such that both the mass matrix for the N_i^c and the charged lepton Yukawa matrix are real and diagonal. Notice that the Z_2 parity prohibits the neutrino Yukawa interactions as $N_i^c L_j H_u$ which give neutrino masses at the tree level, so that the type I seesaw mechanism does not work.

In our model, the neutrino masses are radiatively generated by (I) one-loop diagrams and (II) three-loop diagrams. The one-loop diagrams correspond to the coupling constants y_N^{ij}, and the three-loop diagrams correspond to the coupling constants h_N^{ij}.

A. One-loop contributions

The one-loop diagrams which contribute to the neutrino mass matrix are shown in Fig. 1. These diagrams correspond to the SUSY extension of the Ma model [5]. Such mass terms as η^2 or ζ^2 cannot be written in the superpotential of our model due to the SUSY dynamics at Λ_H, so that the loop diagrams with RH sneutrinos and Z_2-odd fermions do not contribute. The contributions to the mass matrix are calculated as

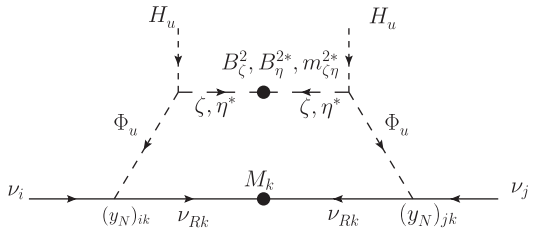

FIG. 1. A one-loop diagram which contributes to the neutrino mass matrix.

$$m_{ij}^{(\mathrm{I})} = \frac{(y_N)^{ki}(y_N)^{kj}}{(4\pi)^2}\{(O_0)^{1\alpha}(O_0)^{1\alpha}M_k - (O_0)^{5\alpha}(O_0)^{5\alpha}M_k\}\bar{B}_0(m_{\Phi_\alpha}^2, M_k^2), \quad (13)$$

where the loop function $\bar{B}_0$ is given as

$$\bar{B}_0(m_1^2, m_2^2) = -\frac{m_1^2 \ln m_1^2 - m_2^2 \ln m_2^2}{m_1^2 - m_2^2}, \quad (14)$$

and the matrix O_0 is the mixing matrix for the Z_2-odd neutral scalars (see Appendix A).

B. Three-loop contributions

The three-loop diagrams which contribute to the neutrino mass matrix are shown in Fig. 2. The contributions are calculated as

$$\begin{aligned} m_{ij}^{(\mathrm{II})} = {} & \frac{\hat{\lambda}^4 v_u^2 (y_E)_i (h_N^*)_{ki} (y_E)_j (h_N^*)_{kj} M_k}{(16\pi^2)^3} \sin^4\beta (U_+^*)_{4\gamma}(U_+)_{4\gamma}(U_+^*)_{4\delta}(U_+)_{4\delta}\{(O_0)_{2\rho}(O_0)_{2\rho} - (O_0)_{6\rho}(O_0)_{6\rho}\} \\ & \times F(M_k^2, m_{\Phi_\rho}^2; m_{e_i}^2, m_{H^\pm}^2, m_{\Phi_\gamma^\pm}^2; m_{e_j}^2, m_{H^\pm}^2, m_{\Phi_\delta^\pm}^2) + \frac{2\hat{\lambda}^2 (y_E)_i (h_N^*)_{ki} (y_E)_j (h_N^*)_{kj} M_k m_{\tilde{\Phi}_\gamma^\pm} m_{\tilde{\Phi}_\delta^\pm}}{(16\pi^2)^3} (V_L^*)_{2\alpha}(V_L)_{2\alpha}(V_L^*)_{2\beta}(V_L)_{2\beta} \\ & \times (U_L^*)_{2\gamma}(U_R)_{2\gamma}(U_L^*)_{2\delta}(U_R)_{2\delta}\{(O_0)_{3\rho}(O_0)_{3\rho} - (O_0)_{7\rho}(O_0)_{7\rho}\} F(M_k^2, m_{\Phi_\rho}^2; m_{\tilde{\chi}_\alpha^\pm}^2, m_{\tilde{e}_{Ri}}^2, m_{\tilde{\Phi}_\gamma^\pm}^2; m_{\tilde{\chi}_\beta^\pm}^2, m_{\tilde{e}_{Rj}}^2, m_{\tilde{\Phi}_\delta^\pm}^2), \end{aligned} \quad (15)$$

where the loop function F is given by [8]

$$\begin{aligned} F(M^2, m_\Phi^2, m_{\chi_1}^2; m_{\phi_1}^2, m_{\Omega_1}^2; m_{\chi_2}^2, m_{\phi_2}^2, m_{\Omega_2}^2) = {} & \frac{(16\pi^2)^3}{i}\int \frac{d^D k}{(2\pi)^D}\frac{1}{k^2 - M^2}\frac{1}{k^2 - m_\Phi^2}\int \frac{d^D p}{(2\pi)^D}\frac{\not{p}}{p^2 - m_{\chi_1}^2}\frac{1}{p^2 - m_{\chi_1}^2}\frac{1}{p^2 - m_{\phi_1}^2} \\ & \times \frac{1}{(k+p_1)^2 - m_{\Omega_1}^2}\int \frac{d^D q}{(2\pi)^D}\frac{(-\not{q})}{(-q)^2 - m_{\chi_2}^2}\frac{1}{(-q)^2 - m_{\phi_2}^2}\frac{1}{(k+(-q))^2 - m_{\Omega_2}^2} \\ = {} & \frac{1}{(M^2 - m_\Phi^2)(m_{\chi_1}^2 - m_{\phi_1}^2)(m_{\chi_2}^2 - m_{\phi_2}^2)}\int_0^\infty k_E^2 d(k_E^2)\left(\frac{M^2}{-k_E^2 - M^2} - \frac{m_\Phi^2}{-k_E^2 - m_\Phi^2}\right) \\ & \times \{\bar{B}_1(-k_E^2, m_{\chi_1}^2, m_{\Omega_1}^2) - \bar{B}_1(-k_E^2, m_{\phi_1}^2, m_{\Omega_1}^2)\} \\ & \times \{\bar{B}_1(-k_E^2, m_{\chi_2}^2, m_{\Omega_2}^2) - \bar{B}_1(-k_E^2, m_{\phi_2}^2, m_{\Omega_2}^2)\}, \end{aligned} \quad (16)$$

with $\bar{B}_1$ being

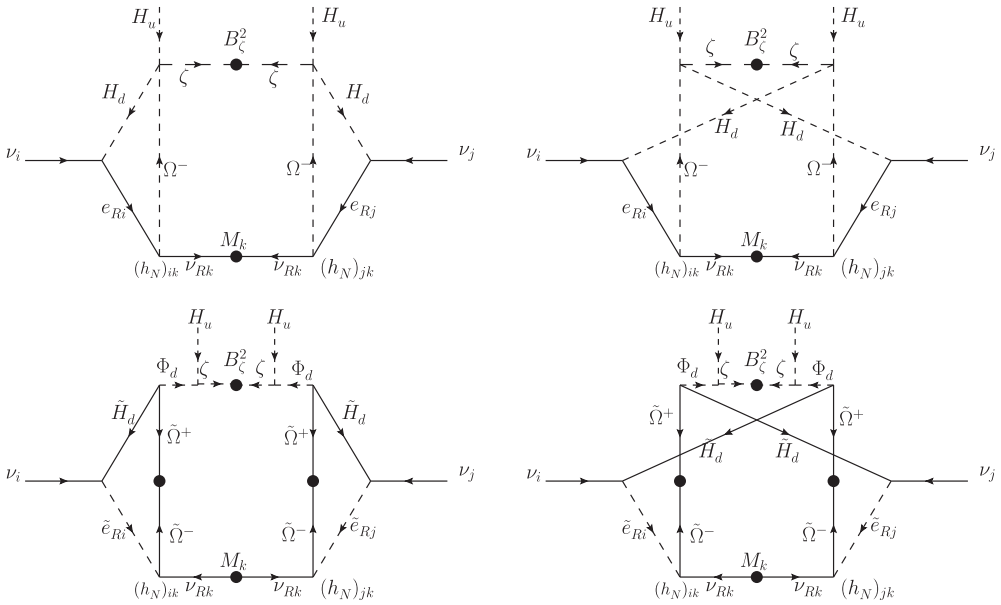

FIG. 2. Three-loop diagrams which contribute to the neutrino mass matrix.

$$\bar{B}_1(p^2, m_1^2, m_2^2) \equiv -\int_0^1 dx x \ln \frac{(1-x)m_1^2 + xm_2^2 - x(1-x)p^2 - i\varepsilon}{\mu^2}. \tag{17}$$

The numerical behavior of the improper integrals in evaluation of the function F is discussed in Ref. [8]. The matrices U_+, U_L, and U_R are mixing matrices for Z_2-odd charged particles as given in Appendix A, while the matrices V_L and V_R are the mixing matrices for the MSSM charginos as

$$V_R^\dagger \begin{pmatrix} M_{\tilde{W}} & \sqrt{2}m_W \cos\beta \\ \sqrt{2}m_W \sin\beta & \mu \end{pmatrix} V_L = \begin{pmatrix} m_{\tilde{\chi}_1} & 0 \\ 0 & m_{\tilde{\chi}_2} \end{pmatrix}, \tag{18}$$

where $M_{\tilde{W}}$ is the wino mass. This is a SUSY extension of the AKS model [7,8].[2] In the AKS model, extra neutral and charged singlet scalar fields are added to a two Higgs doublet model. The chiral superfields ζ and Ω^- correspond to these extra singlet scalar fields. In the SUSY extended AKS model, an extra doublet superfield Φ_d is necessary to provide an indispensable quartic scalar interaction such as $H_u H_d^\dagger \Omega^- \zeta^*$ by F-term. The superfields Φ_u and Ω^+ are required for chiral anomaly cancellation. It is surprising that all the superfields required in the SUSY AKS model are automatically provided in the $\mathrm{SU}(2)_H \times Z_2$ model.

C. Benchmark points

We here consider the benchmark points where the neutrino oscillation data can be reproduced in addition to make 1stOPT strong as $\phi_c/T_c \gtrsim 1$ in the $\mathrm{SU}(2)_H \times Z_2$ model. The calculation of the order of electroweak phase transition, ϕ_c/T_c, is briefly reviewed in Appendix B. In general, both the one-loop and the three-loop diagrams contribute to the neutrino mass generation. However, we here consider the following two limiting cases: (A) one-loop dominant case ($h_N^{ij} = 0$), and (B) three-loop dominant case ($y_N^{ij} = 0$). The definition of the two benchmark points are shown in Table III. The mass of the SM-like Higgs boson is tuned to be $m_h = 125$ GeV by choosing the parameters in the scalar top sector; i.e., SUSY breaking soft masses and left-right mixing parameter of the stops. For simplicity, we do not put any additional flavor mixing in the scalar lepton mass matrices.

We will discuss consequences of the benchmark points. First, we will show the strength of 1stOPT ϕ_c/T_c and related issues in Table IV. In order to satisfy $\phi_c/T_c > 1$ by the mechanism discussed in Refs. [19,20], we take $\hat{\lambda} = 1.8$ which leads to the cutoff scale at around $\Lambda_H = 5$ TeV on both benchmark points. The enhancement occurs by the nondecoupling loop contributions of Z_2-odd scalars. These nondecoupling loop contributions affect the triple coupling of the SM-like Higgs boson λ_{hhh}, and loop effects of Z_2-odd charged scalars can deviate the decay branching ratio of the Higgs boson into diphoton $\mathrm{B}(h \to \gamma\gamma)$ from

[2] In the original non-SUSY AKS model, the Higgs sector is the type-X two Higgs doublet model with neutral and charged singlet fields. The type-X two Higgs doublet model is adopted in order to make the charged Higgs boson light with avoiding too large contribution to the $b \to s\gamma$ process. On the other hand, in the model discussed here, the Z_2-even Higgs sector is the type II two Higgs doublet model and the constraint from $b \to s\gamma$ can be satisfied with the charged Higgs mass taken in the benchmark points. In spite of such a small difference, one can say that the model is essentially identical to the SUSY extended AKS model.

TABLE III. Benchmark parameter set for (A) the one-loop dominant case and (B) three-loop dominant case. For both cases, $B_\Phi = B_\Omega = A_\zeta = A_\eta = A_{\Omega^+} = A_{\Omega^-} = 0$ is taken.

Case	$\hat{\lambda}$	$\tan\beta$	$m_{H^\pm}$	$m_{\tilde{W}}$	μ	μ_Φ	μ_Ω
(A)	1.8	15	350 GeV	500 GeV	100 GeV	550 GeV	−550 GeV
(B)	1.8	30	350 GeV	500 GeV	100 GeV	550 GeV	−550 GeV

Case	$\bar{m}^2_{\Phi_u}$	$\bar{m}^2_{\Phi_d}$	$\bar{m}^2_{\Omega^+}$	$\bar{m}^2_{\Omega^-}$	$\bar{m}^2_\zeta$	$\bar{m}^2_\eta$
(A)	$(100\ \text{GeV})^2$	$(1500\ \text{GeV})^2$	$(1500\ \text{GeV})^2$	$(100\ \text{GeV})^2$	$(1500\ \text{GeV})^2$	$(2000\ \text{GeV})^2$
(B)	$(1500\ \text{GeV})^2$	$(1500\ \text{GeV})^2$	$(1500\ \text{GeV})^2$	$(30\ \text{GeV})^2$	$(1410\ \text{GeV})^2$	$(30\ \text{GeV})^2$

Case	B^2_ζ	B^2_η	$m^2_{\zeta\eta}$
(A)	$(100\ \text{GeV})^2$	$(100\ \text{GeV})^2$	$(100\ \text{GeV})^2$
(B)	$(1400\ \text{GeV})^2$	0	0

Case	M_1	M_2	M_3	$m_{\tilde{\nu}_{R1}}$	$m_{\tilde{\nu}_{R2}}$	$m_{\tilde{\nu}_{R3}}$	$m_{\tilde{e}_{Ri}} (i = 1,2,3)$
(A)	60 GeV	120 GeV	180 GeV	60 GeV	120 GeV	180 GeV	5000 GeV
(B)	100 GeV	2000 GeV	4000 GeV	100 GeV	3000 GeV	5000 GeV	5000 GeV

Case	$(y_N)_{ij}$	$(h_N)_{ij}$
(A)	$\begin{pmatrix} -0.439 & -0.424 & 0.512 \\ 0.226 & 0.218 & -0.263 \\ 0.272 & 1.36 & 1.36 \end{pmatrix} \times 10^{-4}$	$\begin{pmatrix} 0 & 0 & 0 \\ 0 & 0 & 0 \\ 0 & 0 & 0 \end{pmatrix}$
(B)	$\begin{pmatrix} 0 & 0 & 0 \\ 0 & 0 & 0 \\ 0 & 0 & 0 \end{pmatrix}$	$\begin{pmatrix} 0.003 & 0 & 0 \\ -0.0164 - 1.26i & -0.02424 + 0.0049i & -0.0022 + 0.00097i \\ 0.491 - 1.581i & 0.02461 + 0.00537i & 0.0016 + 0.0019i \end{pmatrix}$

the SM prediction. The ratio of λ_{hhh} to its SM prediction and the ratio of $\mathrm{B}(h \to \gamma\gamma)$ to its SM prediction are evaluated for each of the benchmark points as shown in Table IV, and one finds 10%–20% deviations for them.

To see the detail of the nondecoupling effects on the condition of ϕ_c/T_c, λ_{hhh} and $\mathrm{B}(h \to \gamma\gamma)$, we show the mass spectrum of Z_2-odd particles in Table V. In case (A), the spectrum is very similar to the one given in Ref. [20]. There, the charged scalar eigenstate $\Phi_1^\pm$ and $\Phi_2^\pm$ are almost from the charged scalar components of Ω^- and Φ_u, respectively, and their masses are dominated by the $\hat{\lambda}^2 v^2$ terms. So significant nondecoupling effects appear in 1stOPT, λ_{hhh} and $\mathrm{B}(h \to \gamma\gamma)$. In the neutral Z_2-odd scalar sector, there is no significant nondecoupling effects, because all the mass eigenvalues are not dominated by the Higgs VEV contributions.

TABLE IV. The predicted value of the cutoff scale Λ_H, ϕ_c/T_c, the ratio of the coupling constant λ_{hhh} to its SM prediction $\lambda_{hhh}/\lambda_{hhh}|_{\mathrm{SM}}$, and the ratio of the branching ratio $\mathrm{B}(h \to \gamma\gamma)$ to its SM prediction $\mathrm{B}(h \to \gamma\gamma)/\mathrm{B}(h \to \gamma\gamma)|_{\mathrm{SM}}$.

Case	Λ_H	ϕ_c/T_c	$\lambda_{hhh}/\lambda_{hhh}\|_{\mathrm{SM}}$	$\mathrm{B}(h \to \gamma\gamma)/\mathrm{B}(h \to \gamma\gamma)\|_{\mathrm{SM}}$
(A)	5 TeV	1.0	1.18	0.80
(B)	5 TeV	1.2	1.09	0.89

On the other hand, in case (B), the eigenstates Φ_2^0 and Φ_3^0 which are almost from the neutral components of η give significant contributions to ϕ_c/T_c and λ_{hhh}. In addition, the nondecoupling effect by $\Phi_1^\pm \sim \Omega^-$ contributes to ϕ_c/T_c, λ_{hhh} and $\mathrm{B}(h \to \gamma\gamma)$ the same as in case (A).

Next, we will show the neutrino masses and mixing angles obtained on the benchmark points. In order to obtain the neutrino mass scale of order of 0.1 eV, the constants y_N^{ij} in case (A) are $\mathcal{O}(10^{-4})$. On the other hand, in case (B), some elements of h_N^{ij} are required to be rather large. Especially, in order to compensate the suppression by the small electron Yukawa coupling, the magnitudes of couplings h_N^{1i} are of order one. With the coupling constant matrices y_N^{ij} and h_N^{ij} given in Table III, the neutrino mass eigenvalues and the mixing angles are obtained as displayed in Table VI. These predicted values are in the allowed region which is given by the global fitting analysis of neutrino oscillation data as [24]

$$
\begin{aligned}
&2.28 < \frac{|m_3^2 - m_1^2|}{10^{-3}\ \text{eV}^2} < 2.70, \qquad 7.0 < \frac{m_2^2 - m_1^2}{10^{-5}\ \text{eV}^2} < 8.1, \\
&0.27 < \sin^2\theta_{12} < 0.34, \qquad 0.34 < \sin^2\theta_{23} < 0.67, \\
&0.016 < \sin^2\theta_{13} < 0.030,
\end{aligned} \tag{19}
$$

TABLE V. The mass spectrum for the Z_2-odd particles obtained from the benchmark points defined in Table III.

	Z_2-odd neutral bosons							
Case	Φ_1^0	Φ_2^0	Φ_3^0	Φ_4^0	Φ_5^0	Φ_6^0	Φ_7^0	Φ_8^0
(A)	88.3 GeV	88.5 GeV	1457 GeV	1462 GeV	1569 GeV	1571 GeV	2023 GeV	2028 GeV
(B)	126 GeV	294 GeV	294 GeV	1505 GeV	1506 GeV	1525 GeV	1535 GeV	1992 GeV

	Z_2-odd charged bosons			
Case	$\Phi_1^\pm$	$\Phi_2^\pm$	$\Phi_3^\pm$	$\Phi_4^\pm$
(A)	288 GeV	307 GeV	1496 GeV	1517 GeV
(B)	271 GeV	1459 GeV	1506 GeV	1574 GeV

	Z_2-odd neutral fermions			
Case	$\tilde{\Phi}_1^0$	$\tilde{\Phi}_2^0$	$\tilde{\Phi}_3^0$	$\tilde{\Phi}_4^0$
(A)	429 GeV	429 GeV	721 GeV	721 GeV
(B)	422 GeV	422 GeV	725 GeV	725 GeV

	Z_2-odd charged fermions	
Case	$\tilde{\Phi}_1^\pm$	$\tilde{\Phi}_2^\pm$
(A)	429 GeV	721 GeV
(B)	422 GeV	725 GeV

where $m_i (i = 1, 2, 3)$ are the mass eigenvalues of the neutrinos, and θ_{12}, θ_{23}, and θ_{13} are the mixing angles relevant to the solar neutrino mixing, atmospheric neutrino mixing, and the reactor neutrino mixing, respectively.

The coupling constants y_N^{ij} and h_N^{ji} can give significant contributions to some of the lepton flavor violation processes through the RH neutrino and sneutrino mediation diagrams. The predicted values of the branching ratios $\mathrm{B}(\mu \to e\gamma)$ and $\mathrm{B}(\mu \to eee)$ are listed in Table VII. In case (A), as already discussed, the coupling constants y_N^{ij} are so small that the contribution to the $\mu \to e\gamma$ is suppressed enough to satisfy the current upper bound given by the MEG experiment $\mathrm{B}(\mu \to e\gamma) \leq 5.7 \times 10^{-13}$ [25]. In addition, the branching ratio of the $\mu \to eee$ is approximately given as

$$\mathrm{B}(\mu \to eee) \sim \frac{\alpha}{4\pi} \mathrm{B}(\mu \to e\gamma). \tag{20}$$

Then the experimental upper bound on the branching ratio such as $\mathrm{B}(\mu \to eee) \leq 10^{-12}$ [26] is satisfied once the $\mu \to e\gamma$ is suppressed enough. In case (B), on the other hand, large coupling constants h_N^{1i} enhance the $\mu \to e\gamma$ process. The constraint from $\mathrm{B}(\mu \to eee)$ is also severe in this case, even if the branching ratio $\mathrm{B}(\mu \to e\gamma)$ is suppressed enough [10]. It is because the order one coupling constants h_N^{1i} enhance the contributions from box diagram where the RH neutrinos and RH sneutrinos are running in the loop. The predicted values of $\mathrm{B}(\mu \to e\gamma)$ and $\mathrm{B}(\mu \to eee)$ on the benchmark points are shown in Table VII, and we find that they satisfy these experimental upper bounds on both benchmark points. In case (B), since the branching ratio $\mathrm{B}(\mu \to e\gamma)$ is predicted just below the current limit, it is expected that the $\mu \to e\gamma$ process will be observed in future experiments.

We have found that the benchmark points defined in Table III can reproduce the correct values of neutrino masses and mixing angles with satisfying the constraint from lepton flavor violations and with keeping strong enough 1stOPT for electroweak baryogenesis.

TABLE VI. The neutrino masses and mixing angles obtained on the benchmark points defined in Table III.

Case	m_1	m_2	m_3	$\sin^2\theta_{12}$	$\sin^2\theta_{23}$	$\lvert\sin\theta_{13}\rvert$
(A)	0.0 eV	0.0087 eV	0.050 eV	0.31	0.50	0.14
(B)	0.0 eV	0.0084 eV	0.050 eV	0.32	0.50	0.14

TABLE VII. The prediction on the branching ratios of lepton flavor violation processes $\mathrm{B}(\mu \to e\gamma)$ and $\mathrm{B}(\mu \to eee)$ on the benchmark points defined in Table III.

Case	$\mathrm{B}(\mu \to e\gamma)$	$\mathrm{B}(\mu \to eee)$
(A)	5.2×10^{-19}	8.1×10^{-21}
(B)	5.0×10^{-13}	8.5×10^{-13}

D. Collider signatures

In this paper, we do not perform any complete analysis of specific collider signals. We here give some comments, and detailed analysis of collider signatures in our model will be discussed elsewhere.

1. Precise measurements of the Higgs couplings

As shown in Ref. [20], in the parameter region where 1stOPT becomes strong enough for successful electroweak baryogenesis, the nondecoupling effect gives significant contributions to Higgs couplings such as the hhh coupling and the $h\gamma\gamma$ coupling. The directions of deviations for these coupling constants are related to each other. Both couplings can deviate as large as 20% from the SM predictions, which can be tested by future collider experiments. At the LHC, the branching ratio of Higgs to diphoton process will be measured at about 20% accuracy, but the measurement of triple Higgs boson coupling is very challenging. At the High Luminosity LHC with the luminosity of 3000 fb^{-1}, $\text{B}(h \to \gamma\gamma)$ will be measured with 10% accuracy [27]. The triple Higgs boson coupling can be measured at the high luminosity LHC and much better at the international linear collider (ILC). It is expected that the hhh coupling can be measured with the accuracy of about 20% or better at the ILC with $\sqrt{s} = 1$ TeV with 2 ab^{-1} [28].

2. Direct search of the extra particles

There are many extra fields which can provide collider signals in our model. The Z_2-even sector of our model is essentially the same as the nMSSM. Therefore we can expect that the collider signals relevant to the Z_2-even particles are the same as those in the nMSSM which are studied in the literature [29].

Our model is characterized by the Z_2-odd sector, so that the collider signals in this sector are very important. In case (A) of our benchmark points, inert doubletlike scalars are light. Collider signatures of the inert doublet scalars have been studied in the literature [30–32]. The inert doublet scalars are color singlet particles, then it is not easy to discover them at the LHC. Even though they can be fortunately discovered at the LHC, precise determination of their masses and quantum numbers is challenging [30]. On the other hand, the ILC is a very powerful tool to study such noncolored inert doublet particles. At the ILC, the mass of charged inert scalar can be measured in a few GeV accuracy, and the mass of neutral inert scalar can be measured in better than 2 GeV accuracy [32].

In case (B), the Z_2-odd singletlike charged particle is required to be as light as 300 GeV for reconstructing correct neutrino mass scale. As discussed in Ref. [8], such the light singletlike charged particle can be studied at the ILC via the pair production such as $e^+e^- \to \phi_1^+\phi_1^-$. Furthermore, due to the interaction of $N_i^c E_j^c \Omega^-$, the production process such as $e^-e^- \to \phi_1^-\phi_1^-$ is possible. This process will be strong evidence of a three-loop neutrino mass generation mechanism [31]. The process can be detected at the e^-e^- collision option of the ILC or the CLIC [8,31].

In addition, the SUSY extended Higgs sector of this model includes several color singlet SUSY partner fermions of the extra scalars. If such SUSY partner particles are discovered, it discriminates our model from non-SUSY models with radiative seesaw scenarios.

E. Discussions

1. Stability of the scalar potential

Since the Higgs sector consists of four doublet scalar fields and two neutral and two charged singlet scalar fields, the structure of scalar potential is complicated. It is not trivial that the realistic vacuum where the VEVs of scalar fields are $\langle H_u^0 \rangle = \frac{v}{\sqrt{2}} \sin\beta$, $\langle H_d^0 \rangle = \frac{v}{\sqrt{2}} \cos\beta$ and the other scalar fields have no VEVs is on the global minimum of the potential. The stability of the vacuum should be tested. However, the general analysis of stability of the vacuum is too complicated. Here we have done it with an assumption that the spontaneous breaking of electroweak charge and CP symmetry does not occur. As for both benchmark points, we have found that there is no other local minimum of the potential and the realistic vacuum is on the global minimum at the tree level at the zero temperature.

The thermal history of the multiscalar potential can be also complicated. The thermal evolution of the vacuum state has been studied in some extended Higgs sector such as the general two Higgs doublet model [33], the inert doublet model [34], and so on. In general, intermediate phases where Z_2 parity, electromagnetic charge, and/or CP symmetry are broken can appear during the thermal evolution of the Universe, even if the realistic vacuum is on the global minimum at the zero temperature. For the benchmark points, we have checked that the direct transition to the realistic vacuum occurs without passing through the intermediate phases.

2. Evaluation of the baryon asymmetry of the Universe

For baryogenesis, we focus on the strength of 1stOPT which gives a necessary condition for successful electroweak baryogenesis, and we have not numerically evaluated the prediction on the BAU in our scenario. In order to complete the numerical evaluation of the BAU, we should also take care of the CP phases. Since it is known that the CP violation in the SM is too small for getting enough large BAU [35], extra CP phases are also required in addition to the mechanism to enhance 1stOPT. In SUSY models, new sources of the CP violation which can contribute to the generation of the BAU can be introduced [36]. In the literature [37], numerical evaluation of the BAU due to the electroweak baryogenesis in the MSSM is discussed. In principle, we can introduce the CP phases to the model in the similar ways as the papers mentioned above. We then expect to obtain a sufficient amount of BAU, once the strong enough 1stOPT is realized.

3. Dark matter

This model includes an unbroken Z_2 parity, which provides DM candidates. Since the Z_2-odd extra fields except for the RH neutrino have quite strong coupling with the

Higgs bosons, they conflict with the bounds from direct detection experiments of the DM. We choose both benchmark points in such a way that the lightest Z_2-odd particle is the RH neutrino and/or the RH sneutrino. If the R parity is also imposed, the lightest SUSY particle also qualifies as the DM candidate. It leads to a rich possibility of the multicomponent DM scenario [22]. In this paper we do not specify the scenario of DM. Detailed analyses of the relic abundance and the direct detection constraints are performed elsewhere.

4. Mediation mechanism of the SUSY breaking

Due to the nonrenormalization theorem, the neutrino masses are not generated supersymmetric; i.e., soft SUSY breaking terms are necessary for loop induced neutrino mass models. In our model, SUSY breaking terms in the last line of Eq. (11) are essential. These terms are not forbidden by the gauge symmetry, but no relevant terms are in the superpotential given in Eq. (10). It may suggest a specific mediation mechanism for the SUSY breaking. It is a quite interesting point that the neutrino mass generation is a key to explore the mediation mechanism of SUSY breaking in our model.

IV. CONCLUSIONS

We have considered a model based on the SUSY gauge theory with $N_c = 2$ and $N_f = 3$ with an additional exact Z_2 symmetry. By adding Z_2-odd RH neutrinos to the model, we have proposed a concrete model which can be a fundamental theory of a low-energy effective theory with radiative seesaw scenarios and with strong 1stOPT. We have shown that radiative seesaw scenarios can be realized in our model and there can be two types of contributions to the neutrino mass matrix; i.e., by one-loop diagrams and also by three-loop diagrams. These contributions correspond to the SUSY versions of the Ma model and the AKS model, respectively. We have also found out the benchmark point for each contribution, where the neutrino oscillation data are correctly reproduced with satisfying the condition of strong 1stOPT and with satisfying the current experimental constraints. Our model is a candidate of the fundamental theory whose low-energy effective theory provides solutions to three serious problems in the SM; i.e., neutrino mass, DM and baryogenesis by physics at the TeV scale. Our model can be tested at current and future collider experiments.

APPENDIX A: MASS MATRICES AND MIXING MATRICES FOR EXTRA FIELDS

Here we will list the mass terms of Z_2-odd particles which are obtained from the superpotential given by Eq. (10) and the soft SUSY breaking terms given by Eq. (11), and we will define the mixing matrices.

The mass terms for the Z_2 odd neutral scalars are given by

$$\mathcal{L} = -\left(\Phi_u^{\rm even} \quad \zeta^{\rm even} \quad \Phi_d^{\rm even} \quad \eta^{\rm even} \quad \Phi_u^{\rm odd} \quad \zeta^{\rm odd} \quad \Phi_d^{\rm odd} \quad \eta^{\rm odd}\right) M_0^2 \begin{pmatrix} \Phi_u^{\rm even} \\ \zeta^{\rm even} \\ \Phi_d^{\rm even} \\ \eta^{\rm even} \\ \Phi_u^{\rm odd} \\ \zeta^{\rm odd} \\ \Phi_d^{\rm odd} \\ \eta^{\rm odd} \end{pmatrix}, \tag{A1}$$

where the superscripts "even" and "odd" denote the CP-even neutral scalar component and CP-odd neutral scalar component, respectively. The 8×8 mass matrix M_0^2 can be written as

$$M_0^2 = \begin{pmatrix} M_{\varphi\varphi}^2 & M_{\varphi\chi}^2 \\ (M_{\varphi\chi}^2)^T & M_{\chi\chi}^2 \end{pmatrix}, \tag{A2}$$

where the three 4×4 matrices are defined as

$$M_{\varphi\varphi}^2 = \mathrm{Re}\, M_{\phi^0}^2 + \begin{pmatrix} 0 & 0 & 0 & 0 \\ 0 & \mathrm{Re}(B_\zeta^2) & 0 & \mathrm{Re}(m_{\zeta\eta}^2) \\ 0 & 0 & 0 & 0 \\ 0 & \mathrm{Re}(m_{\zeta\eta}^2) & 0 & \mathrm{Re}(B_\eta^2) \end{pmatrix}, \tag{A3}$$

$$M^2_{\chi\chi} = \mathrm{Re}\, M^2_{\phi^0} + \begin{pmatrix} 0 & 0 & 0 & 0 \\ 0 & -\mathrm{Re}(B^2_\zeta) & 0 & \mathrm{Re}(m^2_{\zeta\eta}) \\ 0 & 0 & 0 & 0 \\ 0 & \mathrm{Re}(m^2_{\zeta\eta}) & 0 & -\mathrm{Re}(B^2_\eta) \end{pmatrix}, \tag{A4}$$

$$M^2_{\varphi\chi} = -\mathrm{Im}\, M^2_{\phi^0} + \begin{pmatrix} 0 & 0 & 0 & 0 \\ 0 & -\mathrm{Im}(B^2_\zeta) & 0 & -\mathrm{Im}(m^2_{\zeta\eta}) \\ 0 & 0 & 0 & 0 \\ 0 & \mathrm{Im}(m^2_{\zeta\eta}) & 0 & -\mathrm{Im}(B^2_\eta) \end{pmatrix}, \tag{A5}$$

and

$$M^2_{\varphi^0} = \begin{pmatrix} \bar{m}^2_{\Phi_u} + \hat{\lambda}^2 \frac{v_d^2}{2} + D_{\Phi^0} & \hat{\lambda}^* \mu \frac{v_u}{\sqrt{2}} + A^*_\zeta \frac{v_d}{\sqrt{2}} & -B^*_\Phi \mu^*_\Phi & \hat{\lambda}^* \mu_\Omega \frac{v_d}{\sqrt{2}} - \hat{\lambda} \mu^*_\Phi \frac{v_u}{\sqrt{2}} \\ \hat{\lambda} \mu^* \frac{v_u}{\sqrt{2}} + A_\zeta \frac{v_d}{\sqrt{2}} & \bar{m}^2_\zeta + \hat{\lambda}^2 \frac{v_d^2}{2} & \hat{\lambda} \mu^*_\Phi \frac{v_d}{2} - \hat{\lambda}^* \mu_\Omega \frac{v_u}{\sqrt{2}} & B_\Omega \mu_\Omega \\ -B_\Phi \mu_\Phi & \hat{\lambda}^* \mu_\Phi \frac{v_d}{\sqrt{2}} - \hat{\lambda} \mu^*_\Omega \frac{v_u}{\sqrt{2}} & \bar{m}^2_{\Phi_d} + \hat{\lambda}^2 \frac{v_u^2}{2} - D_{\Phi^0} & -\hat{\lambda} \mu^* \frac{v_d}{\sqrt{2}} - A_\eta \frac{v_u}{\sqrt{2}} \\ \hat{\lambda} \mu^*_\Omega \frac{v_d}{\sqrt{2}} - \hat{\lambda}^* \mu_\Phi \frac{v_u}{\sqrt{2}} & B^*_\Omega \mu^*_\Omega & -\hat{\lambda}^* \mu \frac{v_d}{\sqrt{2}} - A^*_\eta \frac{v_u}{\sqrt{2}} & \bar{m}^2_\eta + \hat{\lambda}^2 \frac{v_u^2}{2} \end{pmatrix}. \tag{A6}$$

The matrix M^2_0 is diagonalized by a real orthogonal matrix O_0 as

$$O^T_0 M^2_0 O_0 = \begin{pmatrix} m^2_{\Phi^0_1} & 0 & 0 & 0 & 0 & 0 & 0 & 0 \\ 0 & m^2_{\Phi^0_2} & 0 & 0 & 0 & 0 & 0 & 0 \\ 0 & 0 & m^2_{\Phi^0_3} & 0 & 0 & 0 & 0 & 0 \\ 0 & 0 & 0 & m^2_{\Phi^0_4} & 0 & 0 & 0 & 0 \\ 0 & 0 & 0 & 0 & m^2_{\Phi^0_5} & 0 & 0 & 0 \\ 0 & 0 & 0 & 0 & 0 & m^2_{\Phi^0_6} & 0 & 0 \\ 0 & 0 & 0 & 0 & 0 & 0 & m^2_{\Phi^0_7} & 0 \\ 0 & 0 & 0 & 0 & 0 & 0 & 0 & m^2_{\Phi^0_8} \end{pmatrix}. \tag{A7}$$

The mass terms for Z_2-odd neutral fermions are written as

$$\mathcal{L} = -\frac{1}{2} (\, \tilde{\Phi}^0_u \quad \tilde{\zeta}^0 \quad \tilde{\Phi}^0_d \quad \tilde{\eta}^0 \,) \tilde{M}_0 \begin{pmatrix} \tilde{\Phi}^0_u \\ \tilde{\zeta}^0 \\ \tilde{\Phi}^0_d \\ \tilde{\eta}^0 \end{pmatrix}, \tag{A8}$$

where the mass matrix is given by

$$\tilde{M}_0 = \begin{pmatrix} 0 & \hat{\lambda} \frac{v_d}{\sqrt{2}} & \mu_\Phi & 0 \\ \hat{\lambda} \frac{v_d}{\sqrt{2}} & 0 & 0 & \mu_\Omega \\ \mu_\Phi & 0 & 0 & -\hat{\lambda} \frac{v_u}{\sqrt{2}} \\ 0 & -\hat{\lambda} \frac{v_u}{\sqrt{2}} & \mu_\Omega & 0 \end{pmatrix}. \tag{A9}$$

The mass matrix $\tilde{M}_0$ can be diagonalized by a unitary matrix $\tilde{U}_0$ as

$$\tilde{U}_0^T \tilde{M}_0 \tilde{U}_0 = \begin{pmatrix} m_{\tilde{\Phi}_1^0} & 0 & 0 & 0 \\ 0 & m_{\tilde{\Phi}_2^0} & 0 & 0 \\ 0 & 0 & m_{\tilde{\Phi}_3^0} & 0 \\ 0 & 0 & 0 & m_{\tilde{\Phi}_4^0} \end{pmatrix}, \tag{A10}$$

and one can obtain the real and positive mass eigenvalues $m_{\tilde{\Phi}_i}$.

The mass terms for the Z_2-odd charged scalars are given by

$$\mathcal{L} = -(\,(\Phi_u^+)^* \quad (\Omega^+)^* \quad \Phi_d^- \quad \Omega^-\,) M_\pm^2 \begin{pmatrix} \Phi_u^+ \\ \Omega^+ \\ (\Phi_d^-)^* \\ (\Omega^-)^* \end{pmatrix}, \tag{A11}$$

with the mass matrix being

$$M_\pm^2 = \begin{pmatrix} \bar{m}_{\Phi_u}^2 + \hat{\lambda}^2 \frac{v_u^2}{2} + D_{\Phi\pm} & \hat{\lambda}\mu_\Phi^* \frac{v_d}{\sqrt{2}} - \hat{\lambda}^* \mu_\Omega \frac{v_u}{\sqrt{2}} & B^* \mu_\Phi^* & \hat{\lambda}^* \mu \frac{v_d}{\sqrt{2}} - A_{\Omega^-}^* \frac{v_u}{\sqrt{2}} \\ \hat{\lambda}^* \mu_\Phi \frac{v_d}{\sqrt{2}} - \hat{\lambda}\mu_\Omega^* \frac{v_u}{\sqrt{2}} & \bar{m}_{\Omega^+}^2 + \hat{\lambda}^2 \frac{v_d^2}{2} + D_{\Omega\pm} & -\hat{\lambda}^* \mu \frac{v_u}{\sqrt{2}} + A_{\Omega^+}^* \frac{v_d}{\sqrt{2}} & B^* \mu_\Omega^* \\ B\mu_\Phi & -\hat{\lambda}\mu^* \frac{v_u}{\sqrt{2}} + A_{\Omega^+} \frac{v_d}{\sqrt{2}} & \bar{m}_{\Phi_d}^2 + \hat{\lambda}^2 \frac{v_d^2}{2} - D_{\Phi\pm} & \hat{\lambda}\mu_\Omega^* \frac{v_d}{\sqrt{2}} - \hat{\lambda}^* \mu_\Phi \frac{v_u}{\sqrt{2}} \\ \hat{\lambda}\mu^* \frac{v_d}{\sqrt{2}} - A_{\Omega^-} \frac{v_u}{\sqrt{2}} & B\mu_\Omega & \hat{\lambda}^* \mu_\Omega \frac{v_d}{\sqrt{2}} - \hat{\lambda}\mu_\Phi^* \frac{v_u}{\sqrt{2}} & \bar{m}_{\Omega^-}^2 + \hat{\lambda}^2 \frac{v_u^2}{2} - D_{\Omega\pm} \end{pmatrix}. \tag{A12}$$

The mass matrix $M_\pm^2$ can be diagonalized by a unitary matrix U_+ as

$$U_+^\dagger M_\pm^2 U_+ = \begin{pmatrix} m_{\Phi_1^\pm}^2 & 0 & 0 & 0 \\ 0 & m_{\Phi_2^\pm}^2 & 0 & 0 \\ 0 & 0 & m_{\Phi_3^\pm}^2 & 0 \\ 0 & 0 & 0 & m_{\Phi_4^\pm}^2 \end{pmatrix}. \tag{A13}$$

The mass terms of the Z_2-odd charged fermions are written as

$$\mathcal{L} = -(\,\tilde{\Phi}_u^+ \quad \tilde{\Omega}^+\,) \tilde{M}_\pm \begin{pmatrix} \tilde{\Phi}_d^- \\ \tilde{\Omega}^- \end{pmatrix}, \tag{A14}$$

where the mass matrix is given by

$$\tilde{M}_\pm = \begin{pmatrix} -\mu_\Phi & \hat{\lambda} \frac{v_u}{\sqrt{2}} \\ -\hat{\lambda} \frac{v_d}{\sqrt{2}} & -\mu_\Omega \end{pmatrix}. \tag{A15}$$

The mass matrix $\tilde{M}_\pm$ is diagonalized by two unitary matrices U_L and U_R as

$$U_R^\dagger \tilde{M}_\pm U_L = \begin{pmatrix} m_{\tilde{\Phi}_1^\pm} & 0 \\ 0 & m_{\tilde{\Phi}_2^\pm} \end{pmatrix}, \tag{A16}$$

where $m_{\tilde{\Phi}_i^\pm}$ are the real and positive mass eigenvalues.

APPENDIX B: CALCULATION OF THE ORDER OF ELECTROWEAK PHASE TRANSITION

In this Appendix, we summarize the calculation of the order of electroweak phase transition, ϕ_c/T_c, which is done by evaluating the one-loop effective potential at finite temperature [38].

For our model, the one-loop effective potential at temperature T is given by

$$V_1(h_u, h_d; T) = V_1^0(h_u, h_d) + \frac{T^4}{2\pi^2}\left[\sum_{i\in Bosons} n_i I_B(m_i(h_u, h_d)^2/T^2) + \sum_{i\in Fermions} n_i I_F(m_j(h_u, h_d)^2/T^2)\right], \quad \text{(B1)}$$

where $V_1^0(h_u, h_d)$ denotes the one-loop effective potential at zero temperature. The functions I_B, I_F are defined as

$$I_B(a) = \int_0^\infty dx x^2 \log\,[1 - \exp(-\sqrt{x^2 + a})], \quad \text{(B2)}$$

$$I_F(a) = \int_0^\infty dx x^2 \log\,[1 + \exp(-\sqrt{x^2 + a})]. \quad \text{(B3)}$$

"Bosons" in the summation include the W and Z bosons as well as the bosonic components of Φ_u, Φ_d, Ω^+, Ω^-, ζ, η. "Fermions" include the top and bottom quarks as well as the fermionic components of Φ_u, Φ_d, Ω^+, Ω^-, ζ, η. Fields other than the above have comparably small coupling constants with the Higgs fields H_u, H_d, so we neglect their contributions. n_i denotes the off-shell degrees of freedom of the field i and $m_i(h_u, h_d)^2$ denotes its field-dependent mass squared that depends on the VEVs of the neutral components of the Higgs fields, h_u, h_d.

In our analysis, we use interpolating functions that approximate the functions I_B, I_F. We numerically evaluate the critical temperature T_c below which h_u, h_d take nonzero values at the absolute minimum of the potential $V_1(h_u, h_d; T)$. The field value at the critical temperature, ϕ_c, is given as $\phi_c = \sqrt{(h_u^C)^2 + (h_d^C)^2}$, where h_u^C, h_d^C denote the values of h_u, h_d at the absolute minimum of the potential $V_1(h_u, h_d; T = T_C)$.

ACKNOWLEDGMENTS

This work was supported in part by Grant-in-Aid for Scientific Research, No. 22244031 (S. K.), No. 23104006 (S. K.), No. 23104011 (T. S.), and No. 24340046 (S. K. and T. S.).

[1] G. Aad *et al.* (ATLAS Collaboration), Phys. Lett. B **716**, 1 (2012); S. Chatrchyan *et al.* (CMS Collaboration), Phys. Lett. B **716**, 30 (2012).
[2] ATLAS Collaboration, Report No. ATLAS-CONF-2013-034; CMS Collaboration, Report No. CMS-PAS-HIG-12-045.
[3] A. Zee, Phys. Lett. **93B**, 389 (1980);**95B**, 461(E) (1980).
[4] A. Zee, Nucl. Phys. **B264**, 99 (1986); K. S. Babu, Phys. Lett. B **203**, 132 (1988).
[5] E. Ma, Phys. Rev. D **73**, 077301 (2006).
[6] L. M. Krauss, S. Nasri, and M. Trodden, Phys. Rev. D **67**, 085002 (2003).
[7] M. Aoki, S. Kanemura, and O. Seto, Phys. Rev. Lett. **102**, 051805 (2009).
[8] M. Aoki, S. Kanemura, and O. Seto, Phys. Rev. D **80**, 033007 (2009).
[9] V. A. Kuzmin, V. A. Rubakov, and M. E. Shaposhnikov, Phys. Lett. **155B**, 36 (1985); A. G. Cohen, D. B. Kaplan, and A. E. Nelson, Annu. Rev. Nucl. Part. Sci. **43**, 27 (1993); M. Quiros, Helv. Phys. Acta **67**, 451 (1994); V. A. Rubakov and M. E. Shaposhnikov, Usp. Fiz. Nauk **166**, 493 (1996) [Phys. Usp. **39**, 461 (1996)]; K. Funakubo, Prog. Theor. Phys. **96**, 475 (1996); M. Trodden, Rev. Mod. Phys. **71**, 1463 (1999); W. Bernreuther, Lect. Notes Phys. **591**, 237 (2002); J. M. Cline, arXiv:hep-ph/0609145 D. E. Morrissey and M. J. Ramsey-Musolf; New J. Phys. **14**, 125003 (2012).
[10] M. Aoki, S. Kanemura, and K. Yagyu, Phys. Rev. D **83**, 075016 (2011).
[11] R. Harnik, G. D. Kribs, D. T. Larson, and H. Murayama, Phys. Rev. D **70**, 015002 (2004).
[12] S. Chang, C. Kilic, and R. Mahbubani, Phys. Rev. D **71**, 015003 (2005); A. Delgado and T. M. P. Tait, J. High Energy Phys. 07 (**2005**) 023.
[13] K. A. Intriligator and N. Seiberg, Nucl. Phys. Proc. Suppl. BC **45**, 1 (1996).
[14] C. Liu, Phys. Rev. D **61**, 115001 (2000); M. A. Luty, J. Terning, and A. K. Grant, Phys. Rev. D **63**, 075001 (2001); H. Murayama, arXiv:hep-ph/0307293; T. Abe and R. Kitano, Phys. Rev. D **88**, 015019 (2013).
[15] S. Kanemura, T. Shindou, and T. Yamada, Phys. Rev. D **86**, 055023 (2012).
[16] C. Panagiotakopoulos and K. Tamvakis, Phys. Lett. B **446**, 224 (1999); **469**, 145 (1999); C. Panagiotakopoulos and A Pilaftsis, Phys. Rev. D **63**, 055003 (2001); A. Dedes, C. Hugonie, S. Moretti, and K. Tamvakis, Phys. Rev. D **63**, 055009 (2001).
[17] S. Kanemura, Y. Okada, and E. Senaha, Phys. Lett. B **606**, 361 (2005).
[18] C. Grojean, G. Servant, and J. D. Wells, Phys. Rev. D **71**, 036001 (2005).

[19] S. Kanemura, E. Senaha, and T. Shindou, Phys. Lett. B **706**, 40 (2011).
[20] S. Kanemura, E. Senaha, T. Shindou, and T. Yamada, J. High Energy Phys. 05 (**2013**) 066.
[21] H. Georgi, A. Manohar, and G. W. Moore, Phys. Lett. **149B**, 234 (1984); H. Georgi and L. Randall, Nucl. Phys. **B276**, 241 (1986); A. Luty, Phys. Rev. D **57**, 1531 (1998); A. G. Cohen, D. B. Kaplan, and A. E. Nelson, Phys. Lett. B **412**, 301 (1997).
[22] F. D'Eramo and J. Thaler, J. High Energy Phys. 06 (**2010**) 109; G. Belanger and J.-C. Park, J. Cosmol. Astropart. Phys. 03 (**2012**) 038; G. Belanger, K. Kannike, A. Pukhov, and M. Raidal, J. Cosmol. Astropart. Phys. 04 (**2012**) 010; M. Aoki, M. Duerr, J. Kubo, and H. Takano, Phys. Rev. D **86**, 076015 (2012); M. Aoki, J. Kubo, and H. Takano, Phys. Rev. D **87**, 116001 (2013).
[23] S. Kanemura, N. Machida, T. Shindou, and T. Yamada (work in progress).
[24] G. L. Fogli, E. Lisi, A. Marrone, D. Montanino, A. Palazzo, and A. M. Rotunno, Phys. Rev. D **86**, 013012 (2012); M. C. Gonzalez-Garcia, M. Maltoni, J. Salvado, and T. Schwetz, J. High Energy Phys. 12 (**2012**) 123.
[25] J. Adam *et al.* (MEG Collaboration), Phys. Rev. Lett. **110**, 201801 (2013).
[26] U. Bellgardt *et al.* (SINDRUM Collaboration), Nucl. Phys. **B299**, 1 (1988).
[27] ATLAS Collaboration, Report No. ATL-PHYS-PUB-2012-001; ATLAS Collaboration, Report No. ATL-PHYS-PUB-2012-004.
[28] H. Baer, T. Barklow, K. Fujii, Y. Gao, A. Hoang, S. Kanemura, J. List, H. E. Logan *et al.*, arXiv:1306.6352.
[29] C. Balazs, M. S. Carena, A. Freitas, and C. E. M. Wagner, J. High Energy Phys. 06 (**2007**) 066; J. Cao, H. E. Logan, and J. M. Yang, Phys. Rev. D **79**, 091701 (2009).
[30] R. Barbieri, L. J. Hall, and V. S. Rychkov, Phys. Rev. D **74**, 015007 (2006); A. Goudelis, B. Herrmann, and O. Stal, J. High Energy Phys. 09 (**2013**) 106; Q.-H. Cao, E. Ma, and G. Rajasekaran, Phys. Rev. D **76**, 095011 (2007); E. Lundstrom, M. Gustafsson, and J. Edsjo, Phys. Rev. D **79**, 035013 (2009); E. Dolle, X. Miao, S. Su, and B. Thomas, Phys. Rev. D **81**, 035003 (2010); X. Miao, S. Su, and B. Thomas, Phys. Rev. D **82**, 035009 (2010); M. Gustafsson, S. Rydbeck, L. Lopez-Honorez, and E. Lundstrom, Phys. Rev. D **86**, 075019 (2012).
[31] M. Aoki and S. Kanemura, Phys. Lett. B **689**, 28 (2010).
[32] M. Aoki, S. Kanemura, and H. Yokoya, Phys. Lett. B **725**, 302 (2013).
[33] I. F. Ginzburg and K. A. Kanishev, Phys. Rev. D **76**, 095013 (2007); I. F. Ginzburg, I. P. Ivanov, and K. A. anishev, Phys. Rev. D **81**, 085031 (2010).
[34] I. F. Ginzburg, K. A. Kanishev, M. Krawczyk, and D. Sokolowska, Phys. Rev. D **82**, 123533 (2010); G. Gil, P. Chankowski, and M. Krawczyk, Phys. Lett. B **717**, 396 (2012).
[35] M. B. Gavela, M. Lozano, J. Orloff, and O. Pene, Nucl. Phys. **B430**, 345 (1994); M. B. Gavela, P. Hernandez, J. Orloff, O. Pene, and C. Quimbay, Nucl. Phys. **B430**, 382 (1994); P. Huet and E. Sather, Phys. Rev. D **51**, 379 (1995).
[36] M. Dine, P. Huet, R. L. Singleton, Jr., and L. Susskind, Phys. Lett. B **257**, 351 (1991); A. G. Cohen and A. E. Nelson, Phys. Lett. B **297**, 111 (1992).
[37] P. Huet and A. E. Nelson, Phys. Rev. D **53**, 4578 (1996); M. S. Carena, M. Quiros, A. Riotto, I. Vilja, and C. E. M. Wagner, Nucl. Phys. **B503**, 387 (1997); J. M. Cline, M. Joyce, and K. Kainulainen, Phys. Lett. B **417**, 79 (1998); A. Riotto Nucl. Phys. **B518**, 339 (1998); Phys. Rev. D **58**, 095009 (1998); M. Trodden, Rev. Mod. Phys. **71**, 1463 (1999); J. M. Cline and K. Kainulainen, Phys. Rev. Lett. **85**, 5519 (2000); J. M. Cline, M. Joyce, and K. Kainulainen, J. High Energy Phys. 07 (**2000**) 018; M. S. Carena, J. M. Moreno, M. Quiros, M. Seco, and C. E. M. Wagner, Nucl. Phys. **B599**, 158 (2001); M. S. Carena, M. Quiros, M. Seco, and C. E. M. Wagner, Nucl. Phys. **B650**, 24 (2003).
[38] L. Dolan and R. Jackiw, Phys. Rev. D **9**, 3320 (1974).